Kinetic Monte Carlo simulation of the effect of coalescence energy release on the size and shape evolution of nanoparticles grown as an aerosol

D. Mukherjee, C. G. Sonwane, and M. R. Zachariah[a)]
Departments of Mechanical Engineering and Chemistry, University of Minnesota, Minneapolis, Minnesota 55455

(Received 28 October 2002; accepted 15 April 2003)

We develop a kinetic Monte Carlo algorithm to describe the growth of nanoparticles by particle–particle collision and subsequent coalescence. The unique feature of the model is its ability to account for the exothermic nature of particle coalescence events and to show how the resulting nonisothermal behavior can be used to change the primary particle size and the onset of aggregation in a growing nanoaerosol. The model shows that under certain conditions of gas pressure, temperature, and particle volume loadings, the energy release from two coalescing nanoparticles is sufficient to cause the particle to exceed the background gas temperature by many hundreds of degrees. This in turn results in an increase in the microscopic transport properties (e.g., atomic diffusivity) and drive the coalescence process even faster. The model compares the characteristic times for coalescence and collision to determine what conditions will lead to enhanced growth rates. The results, which are presented for silicon and titania as representative nanoparticle systems, show that increasing volume loading and decreasing pressure result in higher particle temperatures and enhanced sintering rates. In turn, this results in a delay for the onset of aggregate formation and larger primary particles. These results suggest new strategies for tailoring the microstructure of nanoparticles, through the use of process parameters heretofore not considered as important in determining primary particle size. © *2003 American Institute of Physics*.
[DOI: 10.1063/1.1580098]

INTRODUCTION

The study of the coagulation and coalescence of nanosized aerosols resulting in agglomerate formation and the growth characteristics, morphology and size distributions of primary particles in agglomerates have been an area of extensive study in both theoretical and experimental works. The coalescence of particles resulting in spherical particles can be of importance in predicting the uniformity of particle sizes required for pigment synthesis, chemical vapor deposition, carbon black, etc. On the other hand, clusters of individual primary particles forming aggregates of higher specific surface area are known to enhance catalytic activity[1] or the rate of energy release in propellants.[2] Indeed many thermal, mechanical and optical properties[3] are determined by the size of primary particles. Thus, the ability to predict and control primary particle sizes of nanostructured materials either in the free state or stabilized in an aggregate is of paramount importance in the implementation of many of the technologies that envisage a size-dependent property.

Typically in many aerosol processes, a high concentration of very small particles undergoes rapid coagulation. This may lead to the formation of fractal-like agglomerates consisting of a large number of spherical primary particles of approximately uniform diameter.[4] The size of the primary particles ultimately is determined by the relative rates of particle–particle collision and coalescence of a growing aerosol.[5] At very high temperatures for example, particle coalescence occurs almost on contact, resulting in uniform spherical primary particles of relatively small surface area. At low temperatures, the rate of coalescence may be so slow that particles undergo many collisions, leading to fractal-like agglomerates consisting of very small primary particles and thus large surface area. Of most interest is those intermediate conditions where neither process is rate controlling. Ultimately controlling the coalescence rate is only possible through knowledge of the material properties and the use of a programmed and understood time–temperature history of the growth environment.[6]

There have been other efforts of both experimental and theoretical nature for predicting primary particle sizes for nanoparticles grown from a vapor. These include the study of titania nanoparticle sintering kinetics in free jets and the use of a simple coalescence-collision time crossover model to determine shapes of primary particles;[7,8] TEM observations for Titania primary particle sizes during sintering in heated gas flows;[9] or the analysis of the growth characteristics of silica[10–12] nanoparticles in aerosol reactor cells.[13] Models of nanoparticle coalescence in nonisothermal flames have been developed that employ population balance equations that are variants of the Smoluchowski equation have been developed.[14] Sectional based models for aggregate aerosol dynamics accounting for a gas-phase chemical reaction and sintering have also been developed to determine primary and aggregate particle size distributions under varying reactor temperatures.[10]

a)Corresponding author: Michael R. Zachariah. Electronic mail: mrz@me.umn.edu; Telephone: 612-626-9081; Fax: 612-625-6069.

All the aforementioned works on the prediction of primary particle sizes have been constructed *with the underlying assumption that particles were always at the background gas temperatures*. Freund and Bauer[15] possibly carried out the closest experimental work dealing with energy release during condensation of aerosol clusters for homogeneous nucleation in metal vapors. Certainly on the experimental side, the determination of particle temperature over extremely short time scales, as we will encounter in this work, would require a determined effort to probe this effect.

More recently we showed[6,21] that the coalescence process, which is exothermic in nature, could significantly alter the sintering rate of nanoparticles. Moreover, we showed the very surprising result that background gas pressures and volume loading of the material could significantly change the overall temporal energy balance of coalescing particles, and could be used as process parameters to control primary particle size and the onset of aggregation.[21] The motivation for this discovery was an earlier study by Zachariah and Carrier[17] on the coalescence characteristics of silicon nanoparticles using molecular dynamics (MD) simulation methods. That work showed that when particles coalesce, there is a significant increase in particle temperature. Following collision, the formation of new chemical bonds between particles results in heat release and the formation of a neck between the particles. This heat release may, under some conditions, result in an increase in particle temperature well above the background gas. In the recent papers of Lehtinen and Zachariah,[6,21] it was shown that since these particles coalesce predominantly by a solid-state diffusion mechanism, which is an extremely sensitive function of temperature, the increase in particle temperature itself has an important effect on the coalescence dynamics. In fact, it was shown that for silicon nanoparticle coalescence this effect reduced, in some cases, the coalescence time by several orders of magnitude! *However, these studies did not consider ensemble aerosols effects, which is the subject of this paper*. Here, by ensemble effects we refer to the random collision/coalescence processes between particle/aggregate pairs of any size and shape, where simultaneous coalescence of all the system agglomerates that have undergone collisions at any instant of time are allowed to take place.

Monte Carlo methods have recently been shown to be a useful tool for simulating coagulation–coalescence phenomena. They have the advantage that both length and time scale phenomena can be simultaneously solved without a single unifying governing multivariate equation. Furthermore, Monte Carlo methods provide an intuitive tool in simulating the random coagulation process without any *a priori* assumption of the aerosol size distribution.

Rosner and Yu[18] have used Monte Carlo methods to demonstrate the "self preserving" asymptotic pdf for bivariate populations in free molecular regime. Kruis *et al.*[19] have used Monte Carlo methods to establish its suitability for simulating complex particle dynamics. These works have clearly demonstrated the statistical accuracy of Monte Carlo method by comparing it with the theoretical solutions for aggregation and the asymptotic self-preserving particle-size distribution[5] for coagulation. In a parallel work, Efendiev and Zachariah[20] had recently demonstrated the effectiveness of the method, by developing a hybrid Monte Carlo method for simulating two-component aerosol coagulation and internal phase-segregation.

In this paper we develop a Monte Carlo model on the lines of earlier works of Efendiev and Zachariah[20] to extend their work on particle coagulation by incorporating nonisothermal finite rate coalescence processes. We also investigate the inter-relationships of heat release and coalescence as already proposed by Lehtinen and Zachariah.[6,21] We will use a kinetic Monte Carlo (KMC) method to study the effect of gas temperature, pressure, and material volume loading on the heat release phenomenon during the time evolution of a nanoparticle cloud growing by random collision/coalescence processes. We then analyze their significance in predicting the primary particle growth rates. We describe the role of nonisothermal coalescence process in controlling primary particle growth rates and aggregate formation for typical silicon and titania nanoparticles. As seen by the large body of earlier works, these two materials have been subjects of considerable interest, primarily due to the industrial importance of these particles.

MATHEMATICAL MODEL AND THEORY

Smoluchowski equation and collision kernel formulation

The particle size distribution of a polydisperse aerosol undergoing coagulation can be described by the Smoluchowski equation as

$$\frac{dN(t,V_j)}{dt}=\frac{1}{2}\int_0^{V_j}K(V_i,V_j-V_i)N(t,V_i)N(t,V_j-V_i)dV_i - N(t,V_j)\int_0^{\infty}K(V_j,V_i)N(t,V_i)dV_i, \quad (1)$$

where t is the time, $K(V_i,V_j)=K_{i,j}$ is the kinetic coagulation kernel for the particles chosen with volume V_i and V_j, and $N(t,V_j)$ is the number density of the $\{j\}$ cluster.[5]

The appropriate form of the coagulation or collision kernel depends on the Knudsen size regime of the growth. For our interest, the kernel need only be considered for the free molecule regime and takes the form[5]

$$K_{ij}^F=K^F(V_i,V_j)=\left(\frac{3}{4\pi}\right)^{1/6}\left(\frac{6k_BT_p}{\rho_p}\right)^{1/2}\left(\frac{1}{V_i}+\frac{1}{V_j}\right)^{1/2}(V_i^{1/3}+V_j^{1/3})^2, \quad (2)$$

where, k_B denotes the Boltzmann constant, T_p is the particle temperature considered for collision, and ρ_p is the particle density (assumed constant).

For our purposes one has to bear in mind that in free molecular regime the temperature dependence of the collision kernel ($K_{ij}^F \propto T_p^{1/2}$) arises from the mean thermal speed of the nanoparticles derived from kinetic theory and expressed in the form $\bar{c}_i=(8k_BT_p/\pi\rho_pV_i)^{1/2}$. Although the kernel has a weak dependence on the temperature, in our case the particle temperatures can become significantly higher than the background gas temperature. Thus, while formulating the

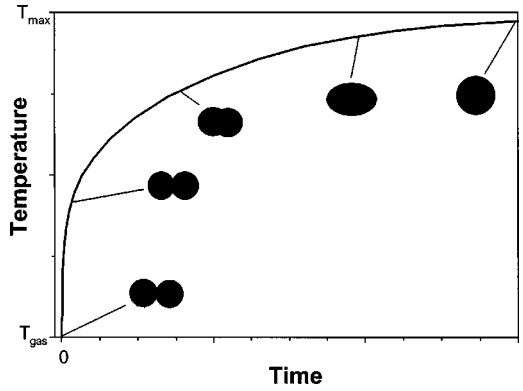

FIG. 1. Schematic representation of the temporal evolution of particle temperature and shape in the nanoparticle coalescence process.

collision kernel, we have considered its dependence on the particle temperature during the coalescence process. Hence, the above collision kernel takes the form

$$K_{ij}^{F}=K^{F}(V_i,V_j) =\left(\frac{3}{4\pi}\right)^{1/6}\left(\frac{6k_{\mathrm{B}}}{\rho_p}\right)^{1/2}\left(\frac{T_i}{V_i}+\frac{T_j}{V_j}\right)^{1/2}(V_i^{1/3}+V_j^{1/3})^2, \quad (3)$$

where T_i and T_j are the respective temperatures of particles in the system considered for collision.

Energy equations for coalescence process

During coalescence, a neck rapidly forms between the particles, which transforms into a spherule, and slowly approaches a sphere coupled with which is the particle temperature rise due to heat release, as demonstrated by Zachariah and Carrier[17] and indicated by the schematic in Fig. 1. Let us consider the case where, based on the collision probabilities, a typical collision event has successfully occurred between two spherical particles of sizes, V_i and V_j. Then upon coagulation it forms a new particle of volume V_i+V_j. It consists of N atoms or units that would essentially undergo the coalescence process and, hence, would be used for formulating the typical energy equations and the corresponding heat release associated with modeling the entire process for all such particles. We assume that the energy E of a particle throughout the coalescence process can be described with bulk and surface contribution terms:[22]

$$E=\underbrace{N_w[\varepsilon_b(0)+c_vT_p]}_{\mathbf{E_{bulk}}}+\underbrace{\sigma_s a_p}_{\mathbf{E_{surf}}}, \quad (4)$$

where a_p is the surface area of the coalescing particle pair, σ_s the surface tension, $\varepsilon_b(0)$ the bulk binding energy (negative) at zero temperature, c_v the constant volume heat capacity (mass specific, J/kg K) and N_w is the equivalent mass (kg) of N atoms in the particle pair undergoing coalescence. Under adiabatic conditions considered over a particle pair, the energy E would be constant, while the coalescence event will result in a decrease in the surface area, a_p and therefore an increase in particle temperature.

Any change in total energy, E, of the particle (or aggregate) can only result from energy loss to the surroundings, by convection, conduction to the surrounding gas, radiation, or evaporation. Thus, for the temporal energy conservation equation for a particle (or, aggregate) we may write

$$\frac{dE}{dt}=N_wc_v\frac{dT_p}{dt}+\sigma_s\frac{da_p}{dt} =-Z_cm_gc_g(T_p-T_g)-\varepsilon\sigma_{\mathrm{SB}}a_p(T_p^4-T_g^4) -\frac{\Delta H_{\mathrm{vap}}}{N_{\mathrm{Av}}}Z_{\mathrm{ev}}, \quad (5)$$

where T_p is the particle temperature, T_g is the gas temperature (K); c_g the mass specific heat capacity, and m_g is the mass of gas molecules (kg). The emissivity of particles is ε, σ_{SB} is the Stefan–Boltzmann constant, ΔH_{vap} is the enthalpy of vaporization (J/mole), and N_{Av} is the Avogadro number. Z_c is the collision rate (s^{-1}) of gas–particle interactions in the free-molecule range, and Z_{ev} is the evaporation rate of surface atoms based on the calculation of the heterogeneous condensation rate (s^{-1}) of atoms on the particle surface.

The second term on the left-hand side of the energy equation (5) is the heat release due to coalescence arising from surface area reduction. The first and second terms on the right-hand side of the equation are heat losses due to collisions with gas molecules, and radiation, respectively, while the last term represents the heat loss due to evaporation from the particle surface.

We evaluate the surface area reduction term in Eq. (5) with the well-known linear rate law[23] for the final stages of coalescence:

$$\frac{da_p}{dt}=-\frac{1}{\tau_f}(a_p-a_{\mathrm{sph}}), \quad (6)$$

where the driving force for area reduction is the area difference between the area of coalescing particles a_p and that of an equivalent volume sphere, a_{sph}. Equation (6) has been widely used to model the entire process from spherical particles in contact to complete coalescence, since the overall sintering stage is rate controlled by the initial growth to a spheroid.[23]

With the substitution we get the nonlinear differential equation for particle temperature as

$$N_wc_v\frac{dT_p}{dt}=\frac{\sigma_s}{\tau_f}(a_p-a_{\mathrm{sph}})-Z_cm_gc_g(T_p-T_g) -\varepsilon\sigma_{\mathrm{SB}}a_p(T_p^4-T_g^4)-\frac{\Delta H_{\mathrm{vap}}}{N_{\mathrm{Av}}}Z_{\mathrm{ev}}, \quad (7)$$

where τ_f is characteristic coalescence, or fusion time defined as

$$\tau_f=\frac{3k_{\mathrm{B}}T_pN}{64\pi\sigma_sD_{\mathrm{eff}}}, \quad \text{where} \quad D_{\mathrm{eff}}=D_{\mathrm{GB}}\left(\frac{\delta}{d_{p(\mathrm{small})}}\right), \quad (8)$$

D_{eff} being the atomic diffusion coefficient that brings in significant nonlinearity in the above equation, as discussed in detail later in this section. The above formulation for D_{eff} is derived based on the earlier works of Wu *et al.*[24] D_{GB} is the solid-state grain boundary diffusion coefficient having the Arrhenius from $D_{\mathrm{GB}}=A\exp(-B/T_p)$, where σ_s is the particle

TABLE I. Thermodynamic and diffusional properties for silicon and titania.

Properties	Silicon	Titania	References
Bulk melting point, T_m (K)	1683	2103	German[44]
Density, ρ_p (kg/m^3)	2330	3840	German;[44] Weast[45]
Solid surface tension, σ_s (J/m^2)	0.9	0.6	German[44]
			Windeler *et al.*[7,8]
Liquid surface tension, σ_l (J/m^2)	⋯	0.34	Xing and Rosner[14]
			Lehtinen and Zachariah[21]
Constant volume heat capacity, c_v (J/kg K)	729	800	German[44]
Heat of vaporization, ΔH_{vap} (J/mole)	384 000	598 712	German;[44] Samsonov[26]
Heat of fusion, L (J/mole)	⋯	47 927	Lehtinen and Zachariah[21]
Diffusion coefficient parameters:			
Pre-exponential factor, A (m^2/s)	4.69×10^{-7}	7.2×10^{-6}	Zachariah and Carrier[17]
			Astier and Vergnon[46]
Activation energy, E_{ac} (kJ/mole)	62.84	286	Zachariah and Carrier[17]
Normalized activation energy, $B=(E_{\text{ac}}/8.31)$ (K)	7562	34416	Astier and Vergnon[46]
Saturation vapor pressure relations:			
Silicon			
$\log_{10} p_s = a + \frac{b}{T_p} + c \log_{10} T_p + dT_p + eT_p^2$ (p_s in mm of Hg; T_p in K)			Yaws[25]
a=315.0687; b=-7.1384×10^{-4}; c=-89.68; d=8.3445×10^{-3} and e=-2.5806×10^{-9}			
Titania			
$\log_{10} p_s = a + \frac{b}{T_p} + cT_p$ (p_s in Pa or, N/m^2; T_p in K)			Samsonov[26]
a=16.20; b=-30361 and c=-0.492×10^{-3}			

surface tension, δ the grain boundary width (Table I), and $d_{p(\text{small})}$ is the diameter of the smallest particle in the coalescing cluster undergoing a grain boundary diffusion process. The logic assumed here is that the smaller particle in any aggregate would coalesce faster into the larger ones, thereby determining the characteristic coalescence time. The values for pre-exponential factor A and activation energy term B are presented in Table I.

Z_c, the gas–particle collision rate (s^{-1}) in the free-molecule regime results in conduction heat loss from the particle to the surrounding gas and is obtained from kinetic theory as

$$Z_c = \frac{p_g a_p}{\sqrt{2\pi m_g k_B T_g}}, \tag{9}$$

where a_p is the area of the coalescing particle pair and, hence, varying in time according to the rate law [Eq. (6)] and p_g is the background gas pressure.

Z_{ev}, the evaporation rate of surface atoms (s^{-1}) is determined by detailed balancing,[47] and evaluated from the kinetic theory based calculation of the heterogeneous condensation rate on particle surface of area at the saturation vapor pressure given as[5]

$$Z_{\text{ev}} = \frac{\alpha_c p_d a_p}{\sqrt{2\pi m k_B T_p}}, \tag{10}$$

where α_c is the accommodation coefficient assumed to be unity, p_d is the saturation vapor pressure over the droplet (spherical particle) and determined from the Kelvin effect.

Thus, for the evaporative heat loss term, we get

$$\frac{\Delta H_{\text{vap}}}{N_{\text{Av}}} Z_{\text{ev}} = \frac{\Delta H_{\text{vap}}}{N_{\text{Av}}} \left(\frac{\alpha_c a_p p_s}{\sqrt{2\pi m k_B T_p}} \right) \exp\left(\frac{4\sigma_s v_m}{d_p k_B T_p} \right), \tag{11}$$

where p_s is the saturation vapor pressure (Pa) over a flat surface at the instantaneous particle temperature during coalescence[25,26] and v_m is the molar volume (m^3/mole). The equations for vapor pressure of Si and TiO_2 used in the present work have been given in Table I. The exponential dependence on particle temperature implies that as the particles heat by coalescence, significant evaporative cooling might take place.

As discussed in the Introduction, the coalescence process reduces the surface area according to the rate law equation given in Eq. (6), which result in surface energy loss. In an adiabatic case all this energy would be partitioned into the internal thermal energy of particles. However, losses to the surroundings will have a significant impact on the particle temperature and therefore its coalescence dynamics. A detailed description of the coalescence dynamics and energy transfer is obtained by numerically solving the coupled equations (6) and (7).

We note that Eq. (7) is highly nonlinear in temperature through the exponential dependence of the solid-state atomic diffusion coefficient D_{GB} in the particle, which is expressed as

$$D_{\text{GB}} = A \exp\left(-\frac{B}{T_p} \right), \tag{12}$$

where A and B are material-dependent constants (Table I). Thus, in typical solid-state sintering, if particle temperature increases due to heat release effects, then lower gas pressures, higher volume loadings (higher collision frequency), and high gas temperatures may result in particle heat generation being larger than heat loss to the surroundings. This, in turn, increases the diffusion coefficient (D_{eff}) reduces the characteristic coalescence time τ_f and, hence, serves to further increase the particle temperature, and so on.

A further complication that may occur during a coalescence event, is that before the resulting particle can relax back to the background gas temperature, it may encounter yet another collision. This would be the case when the characteristic coalescence time is larger than the collision time ($\tau_f > \tau_{\text{coll}}$), thereby generating aggregates. On the other hand, if $\tau_f < \tau_{\text{coll}}$, particles have sufficient time to coalescence and no aggregate is formed. Therefore, the formation of the often-observed aggregate structure is determined by the relative rates of collision and coalescence. However, the heat release from coalescence, if not removed efficiently from the particle, will keep the coalescence time small relative to the collision time and delay the onset of aggregate formation. Our goal is to understand the nonlinear dynamics leading to the formation of aggregates and its effect in terms of growth characteristics of primary particles that go on to form these aggregates.

Effect of lowered melting point of nanoparticles on coalescence

The diffusion mechanism in nanosized particles might differ from bulk diffusion processes and has been previously studied.[17] Although, the phenomenon is not clearly understood, for most practical purposes of this work, one might assume that classical concepts of volume, grain boundary, and surface diffusion are applicable.[24] Grain boundary diffusion has been pointed out as the most significant solid-state diffusion process in polycrystalline nanosized particles,[17,24] though the exact processes for atomic diffusion depend on the crystalline structures of particles.

The diffusion coefficient being very sensitive to the phase (molten or solid), care must be taken to track the phase changes during the growth process. Of particular importance, in the size range of interest, is the size dependence of the melting point of ultrafine particles. We use here the empirical relation approximating the melting point of nanoparticles as[27]

$$T_{\text{mp}}(d_p) = T_m\left[1 - \frac{4}{L\rho_p d_p}\left(\sigma_s - \sigma_1\left(\frac{\rho_p}{\rho_1}\right)^{2/3}\right)\right]. \tag{13}$$

Here, T_m is the bulk melting point, L the latent heat of melting (J/kg), σ_s and σ_1 are the surface tensions (J/m^2), and ρ_p and ρ_1 are the respective solid and liquid phase densities (kg/m^3). The various material property values are presented in Table I.

This effect of lowered melting point on particle coalescence process will turn out to be of importance for the case of titania growth studies to be investigated in this paper, since the growth of these materials is typically conducted in the 1600–2000 K range. The application of Eq. (13) would show that for titania that has a bulk melting point of 2103 K, the melting point drops to about 1913 K at 5 nm and 1100 K for a 1 nm particle. In such a scenario, at typical flame temperatures encountered in experiments, particles may coalesce under a viscous flow mechanism as opposed to a solid-state diffusion mechanism. It also implies that particles may encounter a phase transition during a coalescence event simply due to the energy release process, i.e., $T_p(t) > T_{\text{mp}}(d_p)$.

To take this into account, the diffusion process and corresponding characteristic coalescence times for the TiO_2 case were computed as follows: (1) when $T_p(t) < T_{\text{mp}}(d_p)$, we had assumed a solid-state grain boundary diffusion process to calculate coalescence time, as given by Eqs. (12) and (2) when $T_p(t) > T_{\text{mp}}(d_p)$, a viscous flow mechanism was used[28] as

$$\tau_f = \frac{\mu d_{\text{eff}}}{2\sigma_1}, \tag{14a}$$

where μ is the viscosity at the particle temperature; σ_1 is the liquid surface tension of the particle, and d_{eff} was taken to be proportional to the instantaneous effective particle diameter (V_p/a_p), i.e., $d_{\text{eff}} = 6V_p/a_p$.

The viscosity μ is estimated from empirical relations[29] as a function of particle temperature, T_p, and melting point for the corresponding particle size, $T_{\text{mp}}(d_p)$. The empirical relation for size-dependent viscosity of nanoparticles is given as

$$\mu = 1.8\times 10^{-7}\frac{[M\cdot T_{\text{mp}}(d_p)]^{1/2}\exp\left(\dfrac{L}{RT_p}\right)}{v_m \exp\left[\dfrac{L}{RT_{\text{mp}}(d_p)}\right]}, \tag{14b}$$

where L is the latent heat of fusion/melting (J/mole) (from standard thermodynamic properties), R is the universal gas constant (J/mole K), v_m is the molar volume (m^3/mole), and M is the molar weight (kg/mole).

Radiation heat loss term for nanoparticles: A discussion

Thermal radiation from small particles is a subject of considerable interest and complexity and has been discussed by a number of earlier works.[30–33]

Our prime concern is in the emissivity values needed in Eq. (7) to determine the effect of radiation heat loss in typical nanoparticles. However, unlike bulk materials, for particles smaller than the wavelength of thermal radiation, the emissivity becomes a strong function of the characteristic dimension of the particle.[34] It is well known from Rayleigh scattering theory that the absorption efficiency: $Q_{\text{abs}} \propto X$, where, X is the nondimensional particle size parameter given as $X = \pi d_p/\lambda$, λ being the wavelength of emitted radiation considered. For very fine particles and for the wavelength range of 800 nm or greater (for thermal radiation), the values for absorption efficiency (Q_{abs}) are extremely small (around 10^{-5}–10^{-7}).

Now, from Kirchhoff's law for radiation from spherical particles, $Q_{\text{abs}} = \varepsilon$.[48] Hence, we conclude that emissivity for thermal radiations from nanoparticles in the Rayleigh limit ($d_p \ll \lambda$) are negligible unless we operate at extremely high temperatures. Thus, for all practical purposes, the radiation heat loss term for the present study can be assumed to be negligible and dropped from the energy equation (7) to give its final form as

$$N_w c_v \frac{dT_p}{dt} = \frac{\sigma_s}{\tau_f}(a_p - a_{\text{sph}}) - Z_c m_g c_g (T_p - T_g) - \frac{\Delta H_{\text{vap}}}{N_{\text{Av}}} Z_{\text{ev}}. \tag{15}$$

Nondimensionalization

A convenient nondimensionalization of Eqs. (6) and (15) can be obtained through

$$t^*=\frac{t}{\tau_0};\quad T^*=\frac{T_p-T_g}{T_g};\quad a^*=\frac{a_p-a_{\mathrm{sph}}}{a_{\mathrm{sph}}},\tag{16}$$

resulting in nondimensional form of surface area reduction [Eq. (6)] and energy equation [Eq. (15)] as

$$\frac{da^*}{dt^*}=-\frac{\tau_0}{\tau_f}a^*,\tag{17}$$

and

$$\frac{dT^*}{dt^*}=\left(\frac{E_s}{E_b}\right)\left(\frac{\tau_0}{\tau_f}\right)a^*-\left(\frac{E_g}{E_b}\right)T^*-\left(\frac{E_v}{E_b}\right).\tag{18}$$

Here, $E_s=\sigma_s a_{\mathrm{sph}}$; $E_b=N_w c_v T_g$; $E_g=Z_c m_g c_g T_g \tau_0$, and $E_v=\Delta H_{\mathrm{vap}}/N_{\mathrm{Av}}Z_{\mathrm{ev}}$, where τ_0 is the characteristic coalescence time calculated at gas temperature, T_g. The rest of the notations represent the same parameters as described earlier in the section. Now, using these terms we could define the following nondimensional energy terms as $B_{\mathrm{HG}}=(E_s/E_b)(\tau_0/\tau_f)$; $C_{\mathrm{cond}}=(E_g/E_b)$ and $C_{\mathrm{evap}}=(E_v/E_b)$ representing the *dimensionless heat generation, conductive heat loss, and the evaporative heat loss terms*, respectively.

NUMERICAL MODEL: MONTE CARLO METHOD

It has been shown rigorously by Norris[35] that the Monte Carlo approach approximates the aerosol coagulation equation for the number concentration of particles of any given size as a function of time. Our kinetic Monte Carlo model has been primarily based on the earlier works of Liffman,[36] Smith and Matsoukas,[37] and the recently developed hybrid Monte Carlo method of Efendiev and Zachariah.[20]

A number of Monte Carlo techniques have been developed for simulating the growth of dispersed systems. Of these, the two primary techniques fall into the class of Constant-Number (*Constant-N*) and the Constant-Volume (*Constant-V*) methods. The classical *Constant-V* method samples a constant volume system of particles, and with the advancement of time reduces the number of particles in the sample due to coagulation. This is the same approach as any other time-driven numerical integration and hence it does not offer a uniform statistical accuracy in time. This reduction in the sample usually needs simulation for a large number of initial particles to ensure an acceptable level of accuracy in the results. This might lead to an underutilization of the computational resources.[38] This problem can be overcome by a *Constant-N* method by refilling the empty sites of the particle array in the system, with copies of the surviving particles. This method has been shown to be more efficient, and has been employed by Kostoglou and Konstandopoulos,[38] Smith and Matsoukas,[37] and Efendiev and Zachariah[20] for simulation of particle coagulation.

To overcome this loss of accuracy due to a continuously decreasing particle number arising from coagulation we used a discrete refilling procedure, as proposed by Liffman,[36] in which whenever the particle number dropped to a sufficiently small value (50% of the initial number) the system was replicated. The *Constant-N* approach can be implemented in two general ways. The first approach is to set a time interval Δt and then use Monte Carlo to decide which and how many events will be realized in the specified time interval.[36,39] This essentially amounts to integrating the population balance forward in time and requires discretization of the time step. In the second approach, a single event is chosen to occur and the time is advanced by an appropriate amount to simulate the phenomenon associated with the event.[40,41] This approach does not require explicit time discretization, and has the advantage that the time step, being calculated during the simulation, adjusts itself to the rates of the various processes.

In the present work we employ the second approach for describing particle coagulation, while the first approach is used for simulating particle coalescence, once a coagulation event has been identified. Thus, more precisely, we first identify a single coagulation event to occur for the particles in our system and compute the mean interevent time required ΔT for the next coagulation event to occur. Then, during this time interval, we simulate the coalescence process along with the associated energy release for all the particles in our system. We note for clarity that at any identified interevent time between two successive particle (or, aggregates) collisions, there will be coalescence taking place for other system particles that had collided earlier in time.

It is important to recognize that the mean characteristic collision time ($\tau_{\mathrm{coll}}\approx\tau_c$) essentially signifies the mean time interval that any particular particle (or aggregate) has to wait before it encounters another collision, while the mean interevent time represents the time between any two successive collision events (ΔT) among any two particles (or aggregates) in the system. The latter also becomes our Monte Carlo simulation time step.

Implementation of MC algorithm: Determination of characteristic time scales for coagulation

Let us consider a simulation system with an initial particle concentration of C_0. A choice of the number of particles N_0 that can be efficiently handled in the simulation defines the effective computational volume, $V_0=N_0/C_0$. To connect the simulations to real time, we calculate the interevent time between any two successive collisions or the Monte Carlo time step, ΔT_k as inversely proportional to sum of the rates of all possible events:

$$\Delta T_k=\frac{V_0}{\Sigma_1 R_1}=\frac{2N_0}{C_0\Sigma_{i=1}^{N_{k-1}}\Sigma_{i=1}^{N_{k-1}}K_{ij}^F},\tag{19}$$

where $R_1=K_{ij}$ is the rate of event 1, defined as the coagulation of the pair (i, j), K_{ij} is the coagulation kernel for sizes i and j, and $V_0=N_0/C_0$ is the actual volume represented in the simulation system for particle concentration, C_0, and number of simulation particles, N_0.

For computational time efficiency, we use a mean coagulation probability, $\langle K_{ij}^F\rangle$, defined as

$$\langle K_{ij}^F\rangle=\frac{\Sigma_{i=1}^{N_{k-1}}\Sigma_{j=1}^{N_{k-1}}K_{ij}^F}{N_{k-1}(N_{k-1}-1)}.\tag{20}$$

Hence, the final form for the Monte Carlo time step as

$$\Delta T_k = \frac{2N_0}{C_0 \langle K_{ij}^F \rangle N_{k-1}(N_{k-1}-1)}. \tag{21}$$

Now, for each collision event, we use the interevent time (ΔT_k or, simply, ΔT) determined above, to simulate the coalescence process for *all particles* by integrating the surface area reduction and the energy equations. Then based on the mean values of the area, volume, and temperature of the particles in the system calculated at the end of each Monte-Carlo time step, the mean characteristic collision time (τ_c) in the free molecular regime is estimated from the self-preserving size distribution theory of Friedlander[5] as

$$\tau_c = 3/B, \quad \text{where } B = (\alpha/2)\left(\frac{6k_B\bar{T}_p}{\rho_p}\right)^{1/2}\left(\frac{3}{4\pi}\right)^{1/6}\phi\bar{V}_p^{(-5/6)}, \tag{22}$$

where $\bar{T}_p$ and $\bar{V}_p$ stands for the mean particle temperature and volume, α, a dimensionless constant equal to 6.55,[42] ρ_p is the density of the particle material (assumed to be temperature independent), and ϕ is the material volume loading in the system considered.

Thus, for each of these interevent times ΔT_k, an integration time step Δt for the coalescence process is determined as

$$\Delta t = \frac{\Delta T_k}{n_{\max}}, \tag{23a}$$

and

$$n_{\max} = \frac{\Delta T_k}{\tau_f} \times p, \tag{23b}$$

where $n_{\max}$ is the number of iterative loops for the numerical integration in time; τ_f is the characteristic coalescence time previously defined in Eq. (8) and p is any integer value normally chosen as $p=10$. This method of choosing the numerical time step ensures sufficient discretization of time step to obtain desired resolution for simulating the coalescence process over the particular interevent collision time and characteristic sintering time, both of which are sensitive to size and temperature.

In order to implement the numerical computation, we defined the coagulation probability as

$$p_{ij} = \frac{K_{ij}^F}{K_{\max}^F}, \tag{24}$$

where, $K_{\max}^F$ is the maximum value of the coagulation kernel among all droplets. At each step two particles are randomly selected and a decision is made whether a coagulation event occurs based on p_{ij}. If the event takes place, we calculate the interevent time, ΔT_k, as shown earlier, and go ahead with the coalescence process. As indicated earlier by Smith and Matsoukas[37] as well as Efendiev and Zachariah,[20] this probability should, in principle, be normalized by the sum of all K_{ij} but the choice of $K_{\max}^F$ is commonly employed in order to increase the acceptance rate while maintaining the relative magnitude of probabilities.

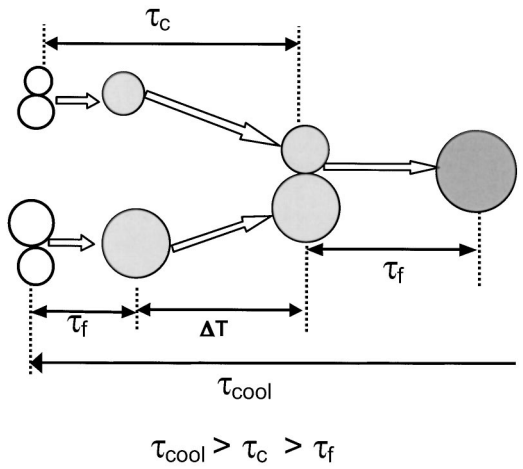

FIG. 2. The schematic diagram indicating the various time scales; mean interevent time (ΔT), characteristic coalescence/fusion (τ_f), characteristic collision (τ_c), and the mean cooling time for particles (τ_{cool}).

In our implementation, a coagulation event occurs only if a random number drawn from a uniform distribution is smaller than the coagulation probability, p_{ij}. If the coagulation is rejected, two new particles are picked and the above steps are repeated until a coagulation condition is met. Upon successful completion of this step the selected particles with volumes V_i and V_j are combined to form a new particle with volume V_i+V_j and the total number of particles in the system is decreased by unity.

When the number of particles due to this repeated coagulation process drops to half of the initial value, we replicate the particles in the system. In order to preserve the physical connection to time, the topping up process must preserve the average behavior of the system like the volume loading or the particle number density corresponding to the time prior to the topping up. In particular, one has to ensure that the interevent time for particle collisions stays the same, and to do this, we increase the effective simulation volume, V_0, in proportion to the increase in the number of particles in the topped up system.

In terms of relating our Monte Carlo simulation to the real physics of the coalescence process, the schematic indicating the role of the different time scales of events is helpful and is shown in Fig. 2. In this figure, one can see that it is the relative magnitudes of the three time scales; the characteristic cooling time (τ_{cool}), characteristic collision time (τ_c), and characteristic coalescence or fusion time (τ_f) that are critical in determining whether a particle colliding would undergo complete sintering, release more heat and grow into a larger uniform primary particle, or would quickly quench and lose heat to form aggregates with larger surface area, but smaller primary particle sizes.

If a criteria is met whereby $\tau_{\text{cool}} > \tau_c > \tau_f$, one should expect to see fully sintered primary particles with large heat release. Whereas, if $\tau_c < \tau_f$, then the particles cannot fully sinter before they encounter the next collision, and this gives rise to the formation of aggregates.

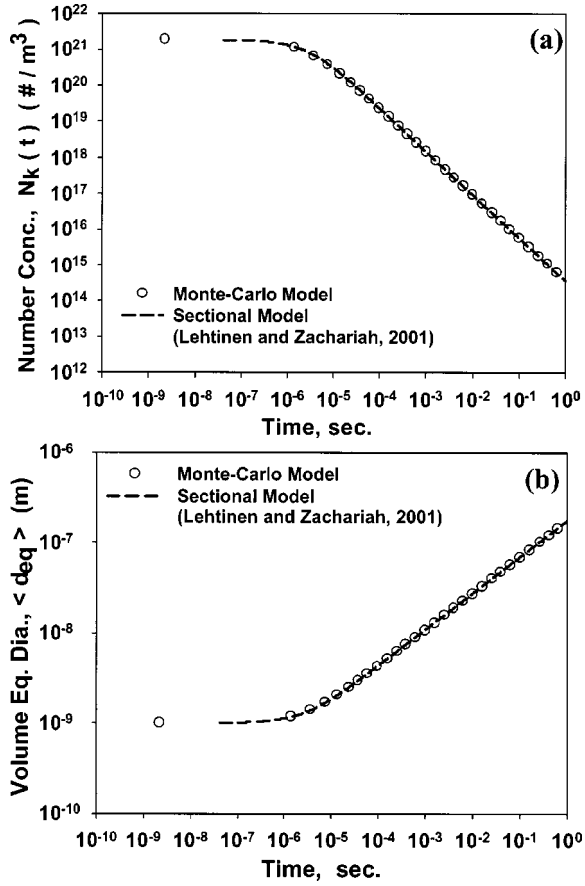

FIG. 3. The variation of (a) particle number concentration and (b) average volume-equivalent diameter with time, as predicted from the Monte Carlo simulation and a sectional model for silicon nanoparticles coagulation (Ref. 16) without any coalescence effects. (Initial diameter= 1 nm, volume loading, $\phi = 10^{-6}$, gas temperature, $T_g = 320$ K, and gas pressure, $P_g = 100$ Pa.)

RESULTS AND DISCUSSION

Validation of the algorithm

In order to estimate the number of particles needed for accurate statistics of the system, we studied the characteristic collision and fusion times, temperature rise, and other properties for two systems consisting of 1000 and 10 000 particles, respectively. Although computation time increases significantly, there is an insignificant change in the mean results for characteristic collision times, fusion times, and particle temperature of these two systems, indicating the attainment of statistical equilibrium. As the plots of T_p versus time as well as τ_f and τ_c versus time for 1000 particle and 10 000 particle systems overlap, results of only a 1000 particle system has been provided. Also, all the results in the present KMC simulation have been obtained by using simulation systems of 1000 particles. It may be recalled here that the use of a topping up technique proposed by Liffman,[36] allows us to reduce the statistical errors in our simulation, even with a smaller number of particles, thereby requiring lesser computer memory.

The average time for a typical simulation of 1000 particles with volume loading of 10^{-4} was anywhere between 15 to 2 hours (depending on the parameters of the case study) on IBM-SP machines at the Minnesota Supercomputing Institute with eight 1.3 GHz power4 processors sharing 16 GB of memory. For ease of scaling, we began our simulation with a monodisperse system of 1 nm diameter. The thermodynamic properties of silicon and titania, such as density, heat capacity, latent heat of fusion/melting, and surface tension were assumed to be particle size independent,[12,22] and are reported in Table I. In most of the simulations studied here, it was found that the increase in background gas temperature due to heat release from coalescence is insignificant and, hence, gas temperature was assumed to be constant throughout.

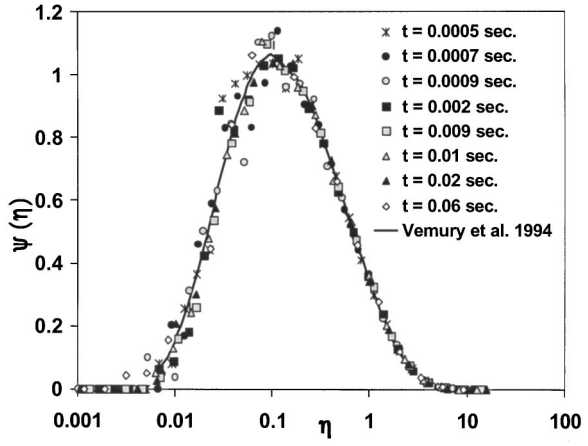

FIG. 4. Self-preserving size distribution for coagulation from the Monte Carlo method compared with the numerical results of Vemury *et al*. (Ref. 43) and plotted as the dimensionless number density, $\psi(\eta) = N(t,V_p)\bar{V}_p/N_\infty$ versus dimensionless volume, $\eta = V_p/\bar{V}_p$. Silicon at $T_g = 320$ K was considered assuming a free molecular regime collision kernel.

The Monte Carlo coagulation algorithm and its accuracy were found to be in excellent agreement with a sectional model simulation,[16] as shown in Figs. 3(a) and 3(b). In addition, as seen in Fig. 4, the particle size distributions at long times, when compared with the numerical results of Vemury *et al*.,[43] showed very good agreement with the known self-preserving size distribution seen for coagulating aerosols.

Effect of background gas temperature

The competing effects of heat release and bath gas cooling were assessed with simulations for silicon nanoparticle growth carried out at gas temperatures of 325, 500, and 800 K with background gas pressure, $P_g = 100$ Pa, and material volume loading, $\phi = 10^{-6}$. Shown in Fig. 5 are plots of the characteristic collision and coalescence times as a function of growth time. Such a plot has been proposed by Windeler *et al*.[7] to assess the competition between these two times and their crossing point. The heavy dotted line represents the characteristic collision time, which is relatively independent of temperature and increases in time for a coagulation process because of the net decrease in particle number concentration. The coalescence time is a function of particle size and temperature, as discussed before. For the work considered here, the coalescence energy release and the losses to the surrounding can significantly alter this time. The crossing point, as suggested by Windeler *et al*., defines the onset of aggregation and enables primary particle size prediction.

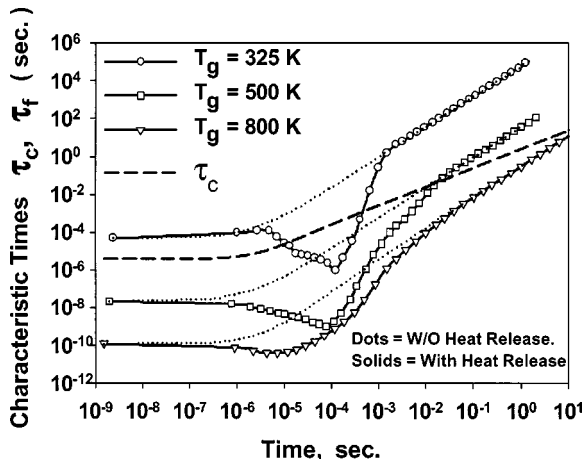

FIG. 5. Variation of characteristic fusion (τ_f) and collision (τ_c) times with residence time for various background gas temperatures for silicon (gas pressure, $P_g = 100$ Pa and volume loading, $\phi = 10^{-6}$).

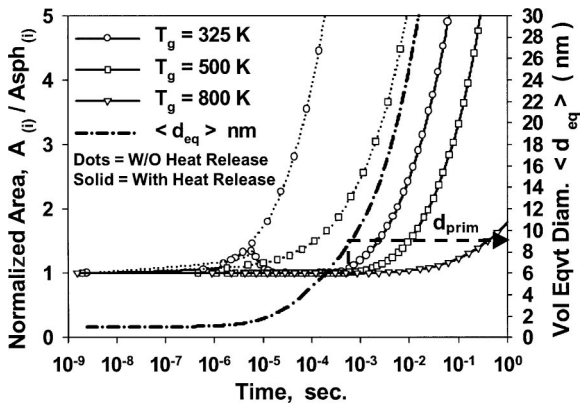

FIG. 7. Variation of silicon normalized area and mean volume equivalent diameter with residence time for various background gas temperatures, T_g, $P_g = 100$ Pa, and particle volume loading, $\phi = 10^{-6}$ ($A_{(i)}$: *particle area* and $A_{sph(i)}$: *equivalent spherical area of the corresponding particle*).

However, we show later that the use of the crossing point between τ_f and τ_c to predict primary particle sizes might not be universally applicable. For the various gas temperatures studied here, we found that with increasing residence time, τ_f initially decreases, reaches a minimum, and then monotonically increases. The decrease in the characteristic coalescence (fusion) time τ_f is actually associated with an increase in the particle temperature and is shown in Fig. 6. Here we see that the particle temperature takes an abrupt and very rapid rise to a value well in excess of 1200 K. This is an indication that the characteristic cooling time under these conditions is slow relative to the fusion time, τ_f, implying larger heat generation. Higher background temperatures show an earlier onset of elevated temperatures and a prolonged dwell time at higher temperatures due to the lower driving force for cooling. At the same time, the delayed onset of heat release effects generate larger aggregates trying to coalesce fully, which causes a stronger driving force for the heat generation arising from the surface area reduction term and, hence, an increase in the net rise in particle temperature. Referring back to Fig. 5, we see that the minimum in the coalescence time roughly corresponds to the peak particle temperature achieved. Also, with increasing gas temperatures, for the same particle size distribution, the relative values of τ_f decrease but τ_c remains relatively unchanged. In the context of our discussion of the comparison of characteristic times, we see from Figs. 5 and 6 that after the initial drop the coalescence time eventually rises, coupled with heat loss from particles, until it crosses the collision time curve. At this point one can reasonably conclude that aggregate formation has been triggered. Beyond this, in the region where $\tau_f > \tau_c$, the particles do not get sufficient time to fully sinter before the next collision takes place thereby forming aggregates. Eventually, the particles get sufficiently larger so that their heat capacity is large enough as to negate any significant temperature rise associated with coalescence and the growing particles return to the background temperature.

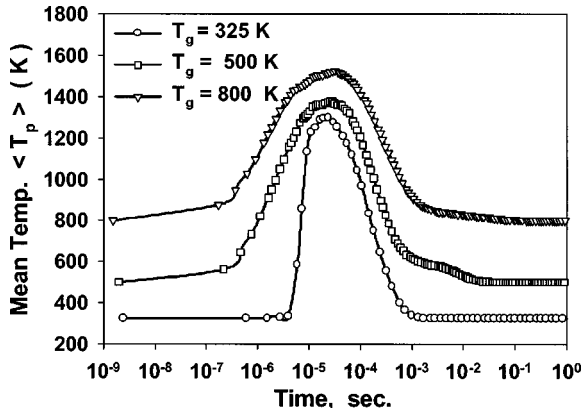

FIG. 6. Variation of mean silicon particle temperature ($\langle T_p \rangle$) with residence time for various background gas temperatures, T_g, at constant gas pressure, $P_g = 100$ Pa, and particle volume loading, $\phi = 10^{-6}$.

The effect on primary particle size, surface area, and the onset of aggregation are illustrated in Fig. 7. In this figure, we plot the normalized surface area $A_{(i)}/A_{sph(i)}$ (or, A/A_{sph}), which is the actual surface area (a_p) to that of the volume equivalent sphere (a_{sph}) as a function of time. It is to be noted here that the notation $A_{(i)}/A_{sph(i)}$ (or, A/A_{sph}) for normalized area used in all plots and discussions in the present work is equivalent to the notation a_p/a_{sph}, as used earlier in the theory. Values of A/A_{sph} larger than unity are a first indication of aggregate formation (i.e., $A/A_{sph} = 1$ implies spheres; $A/A_{sph} > 1$ indicates agglomerate formation). Also plotted is the volume equivalent diameter, d_{eq} (under the assumption of spherical geometry). Primary particle sizes can be estimated at the onset of aggregation by moving vertically from the point where the surface area curve just begins to deviate from unity to the corresponding point on the volume-equivalent diameter curve. From Fig. 7, one can clearly see that the delayed onset (in time) of aggregate formation also implies larger primary particle size and lower surface area.

The effect of heat release on primary particle sizes can be seen by turning off the energy equations solver and assuming that particles are always at the background gas temperature. This essentially implies coalescence without any heat release effects, which is also indicated as the respective dotted lines for τ_f in Fig. 5 and for A/A_{sph} in Fig. 7. We see

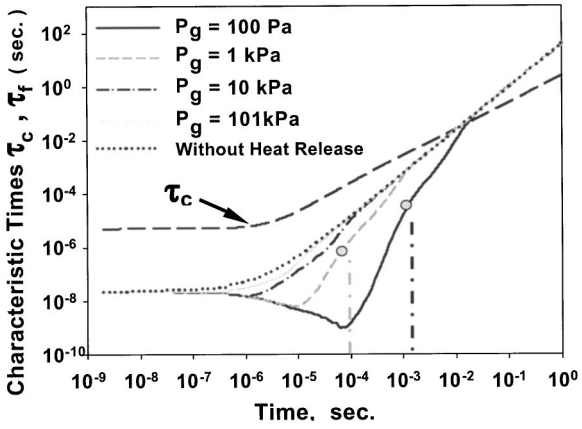

FIG. 8. Variation of characteristic coalescence/fusion (τ_f) and characteristic collision (τ_c) times with residence time for various background gas pressures, P_g , $T_g = 500$ K and particle volume loading, $\phi = 10^{-6}$. A gray point marks the gradient change for τ_f corresponding to the point where $A/A_{\text{sph}} \geq 1$. Results are for silicon.

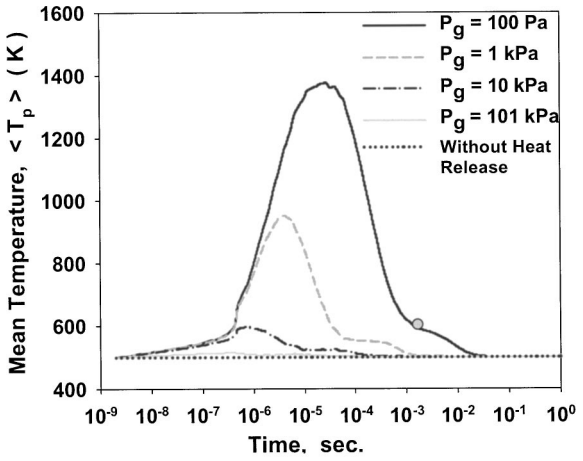

FIG. 9. The variation of mean silicon particle temperature ($\langle T_p \rangle$) with residence time for various background gas pressures, P_g , $T_g = 500$ K, and particle volume loading, $\phi = 10^{-6}$. A gray point marks the gradient change for τ_f corresponding to the point where $A_{(i)}/A_{\text{sph}(i)} \geq 1$.

that without heat release, the characteristic fusion time becomes a monotonically increasing function of time associated with particle growth and does not undergo the sudden decrease in fusion time or enhanced coalescence rate associated with heat release. The effect is most important for the 325 K case, where without heat release no coalescence would take place as seen by the fact that τ_f is always greater than τ_c and A/A_{sph} deviates from unity almost immediately, implying the formation of aggregates with 1 nm primary particles, while with heat release we predict 9 nm primary particle sizes (see Figs. 5 and 7).

It is possible that with higher temperatures as $d\tau_f/dt$ approaches $d\tau_c/dt$ (at the crossing point, i.e., $\tau_f \approx \tau_c$), oblong particles with long necks and strong bonds are formed that would eventually go on to form aggregates. However, at lower temperature the crossing occurs within the heat generation regime and $d\tau_f/dt \gg d\tau_c/dt$ (at $\tau_f \approx \tau_c$). Thus, in this case, uniform spherical particles held together by weak van der Waals' forces in the agglomerates are formed. This theory was also found to be consistent with the earlier work of Windeler *et al.*[7]

Effect of background gas pressure

The conventional wisdom has held that background gas pressure has no role in the heat transfer during the collision/coalescence process. This presumption has held sway because until very recently prior work had neglected the exothermic nature of coalescence. Lehtinen and Zachariah[6,21] were the first to recognize this effect and conclude that gas pressure P_g should have an impact on primary particle size.

The effect of P_g on τ_f at a constant gas temperature for silicon ($T_g = 500$ K, $\phi = 10^{-6}$) is shown in Fig. 8. The corresponding mean particle temperatures are shown in Fig. 9. At 10 kPa, the effect of heat release is negligible as the heat losses to the surroundings are evidently sufficiently facile. As one decreases the pressure, however, the lowered heat loss term through conduction enables the particles to experience elevated temperatures. In these cases the lower the pressure the higher the particle temperatures. This self-heating is also reflected in the lowering of the characteristic sintering time seen in Fig. 8. We estimate the primary particle size (d_{prim}) from the normalized area term ($A/A_{\text{sph}} > 1$) and the corresponding volume-equivalent diameter, as discussed earlier (not shown here) at the point of agglomeration. These results are presented in Fig. 10. At the highest pressure simulated the role of heat release is unimportant, while with decreasing pressure we see a monotonic increase in primary particle size from roughly about 3 nm at 101 kPa to 13 nm 100 Pa. This increase clearly establishes the effect of gas pressure on the primary particle growth rates and, as seen from Fig. 9, reflects the higher particle temperatures experienced at lower pressures resulting from a lower heat loss rate by conduction. It is clearly noticed that the fusion and collision times presented in Fig. 8 show a crossing point independent of pressure! This result indicates that the crossing point may not be the best criteria for assessing the spherical primary particle size, especially beyond the heat generation regime where the relative gradients of the characteristic times, i.e., $d\tau_f/dt$ and

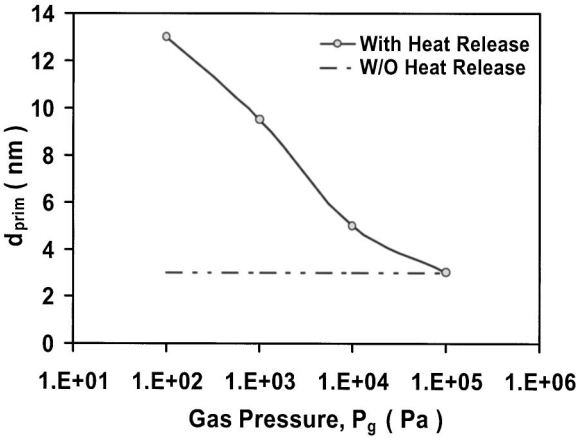

FIG. 10. The effect of background gas pressures (P_g) on primary particle size (d_{prim}) for silicon nanoparticles at constant gas temperature, $T_g = 500$ K and particle volume loading, $\phi = 10^{-6}$. The primary particle size predicted without a heat release effect has also been indicated.

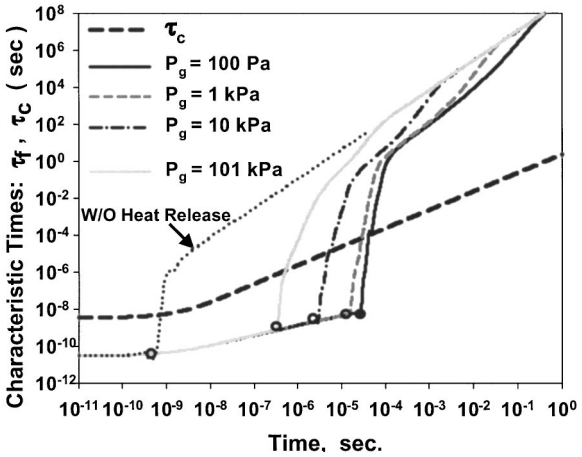

FIG. 11. The variation of characteristic fusion (τ_f) and characteristic collision (τ_c) times with residence time in titania nanoparticle coalescence for various background gas pressures, P_g, $T_g = 1600$ K, and particle volume loading, $\phi = 10^{-3}$. An open circle indicates an abrupt change in the gradient of τ_f corresponding to the phase change from molten to solid state.

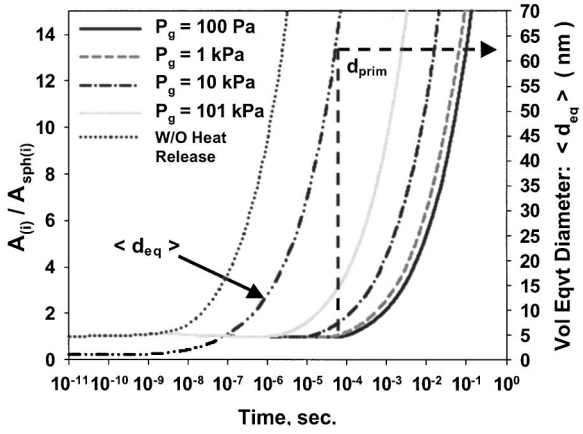

FIG. 12. The effect of background gas pressures (P_g) on the variation of normalized area ($A_{(i)}/A_{\mathrm{sph}(i)}$) and mean volume-equivalent diameter ($\langle d_{\mathrm{eq}} \rangle$) with residence time for titania nanoparticle coalescence at $T_g = 1600$ K and particle volume loading, $\phi = 10^{-3}$. d_{prim} is the primary particle size estimated from the $\langle d_{\mathrm{eq}} \rangle$ value corresponding to $A_{(i)}/A_{\mathrm{sph}(i)} \geqslant 1$ ($A_{(i)}$: *particle area* and $A_{\mathrm{sph}(i)}$: *equivalent spherical area of a corresponding particle*).

$d\tau_c/dt$ at the crossing point are close to each. The two gray points in Fig. 8 mark a noticeable change in $d\tau_f/dt$, indicating the time where the normalized surface area deviates from unity ($A/A_{\mathrm{sph}} > 1$), and was used for determining the spherical primary particle sizes. Beyond this point, and before the particles are agglomerated (i.e., the crossing point between τ_f and τ_c) the primary particles are nonspherical (possibly oblong with large necks) mainly due to the slow crossing point of τ_f and τ_c, as discussed in details earlier.[7]

We also applied the model to titania nanoparticles for different gas pressures ($P_g = 100$ Pa and 1, 10, and 101 kPa) at $T_g = 1600$ K. We choose this example because the operating temperature is one used in industry for the production of titania. It should noted here that the present simulation of particle growth rates due to coalescence has been initiated from the time precursor reactions leading to 100% conversion of precursors (TiC_4 or, TTIP) to titania nanoparticles have been achieved, so that we have a sufficiently large particle number concentration and growth rates are purely due to collision/coalescence process without any nucleation effects. The results illustrate the role of phase transition on growth along with the effect of the size-dependent melting point of nanoparticles. We rely on Eq. (13) to determine, for a given particle, if we are above or below the melting point at any instant in the coalescence process and use the appropriate sintering model (solid-state or viscous flow). This becomes essential since viscous flow characteristic times are two to three orders of magnitude lower than that for solid-state diffusion.

The plot of τ_f and τ_c versus residence time at different pressures for titania is shown in Fig. 11. Initially for small particle sizes (1 nm) $T_p(t) > T_{\mathrm{mp}}(d_p)$ [from Eq. (13)], particles are in a molten state and, hence, characteristic coalescence time (τ_f) is very small so that particles coalesce almost instantly on contact. But as particle sizes increase due to coagulation/coalescence, the corresponding melting point also increases and rises above the particle temperature, i.e., $T_p(t) < T_{\mathrm{mp}}(d_p)$ and the particles shift over to the much slower solid-state diffusion mechanism. In Fig. 11, we indicate this change in phase and diffusion mechanism with the large dots. Beyond these marked points in Fig. 11, τ_f increases with a sharper gradient due to the strong exponential dependence of a solid-state diffusion coefficient on particle temperature, as discussed earlier.

Consistent with our previous discussion relating to the silicon case, we see the significance of $d\tau_f/dt$ and $d\tau_c/dt$ at the crossover point ($\tau_f = \tau_c$) in predicting spherical or nonspherical particles. As seen from Fig. 11, at the crossing point $d\tau_f/dt \gg d\tau_c/dt$ for all the pressures in 100 Pa–101 kPa, which implies primary particles being uniformly spherical[8] at the crossover point. One should also note that the crossing points between τ_f and τ_c are well within the heat generation regime during the solid-state coalescence process. We see that at the time of crossover between τ_f and τ_c for all the pressures (100 Pa–101 kPa) in Fig. 11, the normalized area (A/A_{sph}) plotted in Fig. 12 exceeds unity ($A/A_{\mathrm{sph}} > 1$).

From Fig. 13, it can be seen that in the region of a viscous diffusion mechanism, gas pressures between 1–101 kPa do not significantly affect the maximum particle temperature rise. However, in a solid-state diffusion region, the particle temperatures are higher at lower gas pressure due to lesser heat loss, resulting in a prolonged and enhanced sintering mechanism over the time frame studied that competes with the heat loss terms in the energy balance. In Figs. 11 and 13, the noticeable changes in the gradients of temperature decrease and fusion time increase are due to different regions of heat loss wherein initially particles undergo rapid evaporative cooling and then, once below their size-dependent melting points, the heat loss slows down to conductive losses only. Finally, they cool down to background gas temperature indicated by the merging of all the fusion time gradients where τ_f increases purely due to aggregate growth. Figure 14 illustrates the spherical primary particle sizes as function of different gas pressures and shows that

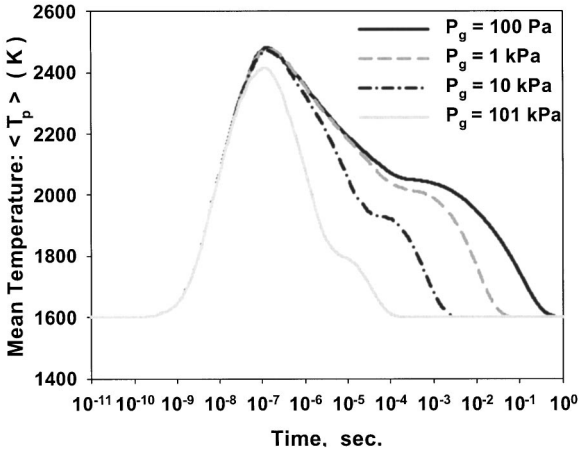

FIG. 13. The variation of the mean particle temperature ($\langle T_p \rangle$) with residence time for various background gas pressures, P_g, $T_g = 1600$ K, and particle volume loading, $\phi = 10^{-3}$ for titania nanoparticle coalescence.

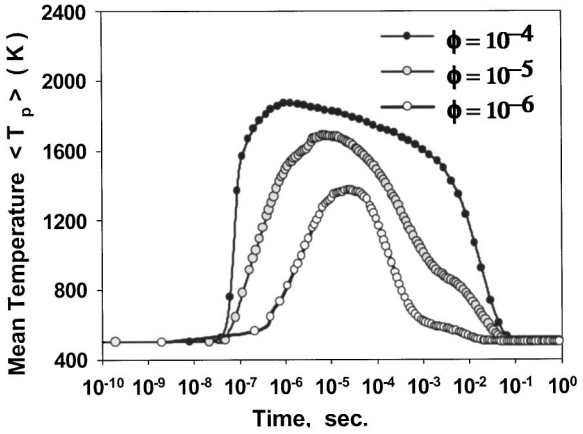

FIG. 15. The effect of different particle volume loading ($\phi = 10^{-4}, 10^{-5}, 10^{-6}$) on the temporal variation of the mean particle temperature ($\langle T_p \rangle$) at constant gas temperature $T_g = 500$ K and gas pressure $P_g = 100$ Pa for silicon particle coalescence.

background pressure can be used to alter the primary particle size.

Effect of volume loading

Volume loading is another important parameter that has been neglected in studies of the primary particle size prediction for nanoparticle coalescence processes. Common laboratory experiments are usually limited to low volume fractions ($\phi = 10^{-6}$) for the ease of experimentation, particularly for those who use *insitu* optical probes. Industrial practice of course seeks to maximize the production rate and typically operates at much higher volume fractions ($\phi = 10^{-3}$). Without the consideration of the exothermic nature of coalescence, it is natural to expect no role for the volume fraction. On the other hand, with heat release considered we might expect that under rapid coalescence conditions, where heat release is faster than energy loss to the surroundings, a higher collision rate might magnify the effect.

The model has been applied to various laboratory and industrial volume loadings in the range of $\phi = 10^{-6}$ to 10^{-3} for silicon (Figs. 15 and 16) and titania (Figs. 17 and 18). The silicon example is most reflective of what might occur in low-pressure plasma, while the titania example is taken to represent an atmospheric pressure flame. For the case of silicon (Fig. 15) we see that all volume loading considered result in elevated particle temperatures, however, increased volume fraction results in higher temperatures for a prolonged time period. This reflects the fact that if the characteristic fusion time is much less than the collision time, there is opportunity to enhance the coalescence process by increasing the collision rate through larger volume loading. In doing so, one essentially enhances the heat release rate by shortening the time interval between the process of cooling that a sintered particle undergoes and another collision that it encounters before cooling down completely, thereby heating up the particle even more. The corresponding primary particle sizes predicted for various volume loadings are seen in Fig. 16. It clearly shows enhanced primary particle sizes as volume loading is increased. We see from Fig. 17 that the titania results are similar, although in this case typical laboratory

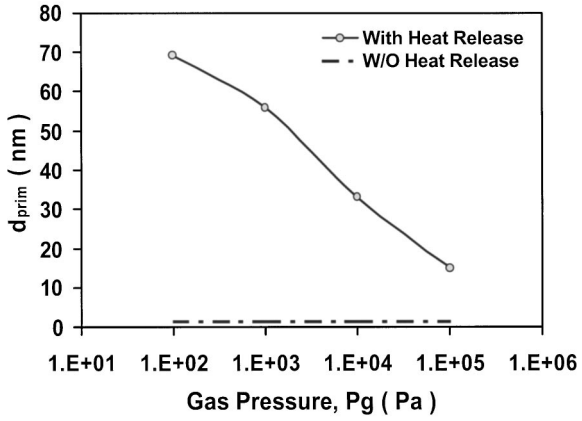

FIG. 14. The effect of background gas pressures (P_g) on primary particle sizes (d_{prim}) for titania nanoparticle coalescence at $T_g = 1600$ K, and particle volume loading, $\phi = 10^{-3}$. Primary particle size without the heat release effect has also been indicated.

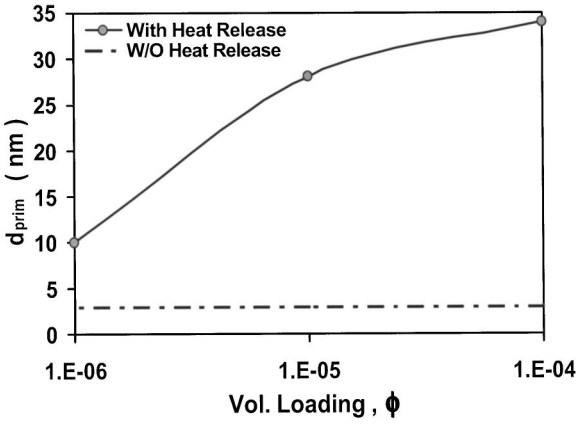

FIG. 16. The effect of particle volume loading ($\phi = 10^{-4}, 10^{-5}, 10^{-6}$) on the prediction of primary particle sizes (d_{prim}) for silicon nanoparticle coalescence $T_g = 500$ K and gas pressure, $P_g = 100$ Pa. Primary particle size predicted without heat release effect has also been indicated.

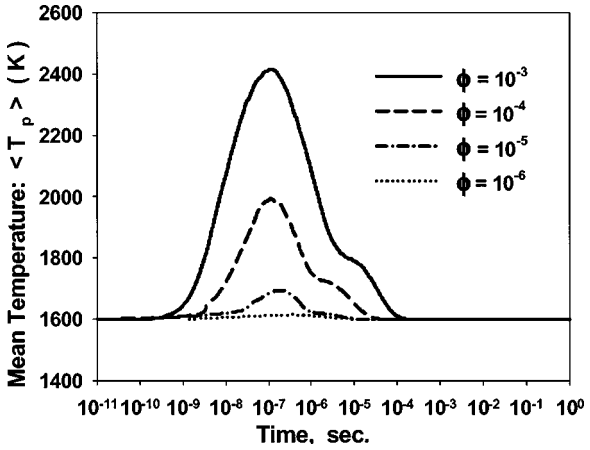

FIG. 17. The effect of different particle volume loading ($\phi = 10^{-3}, 10^{-4}, 10^{-5}, 10^{-6}$) on the temporal variation of mean particle temperature ($\langle T_p \rangle$), $T_g = 1600$ K and gas pressure, $P_g = 101$ kPa (1 atm) for titania nanoparticle coalescence.

conditions ($\phi = 10^{-6}$) do not show any heat release, while loadings more closely approximating industrial practice ($\phi = 10^{-3} - 10^{-4}$) show a large temperature deviation, particularly for the case of volume fraction of 10^{-3}. In turn, and as seen in Fig. 18, higher volume loadings yields larger primary particles.

CONCLUSIONS

In this paper we develop and implement a more generalized version of the earlier works of Lehtinen and Zachariah[6,21] on a nanoparticle coalescence study with the development of a kinetic Monte Carlo model. The kinetic Monte Carlo model presented in this paper is able to account for the ensemble effects of nanoparticle collision/coalescence phenomenon, without any *a priori* constraint on the particle size distribution. In addition, the model has the unique feature that it accounts for the previously ignored physics, mainly that of the exothermic nature of coalescence processes.

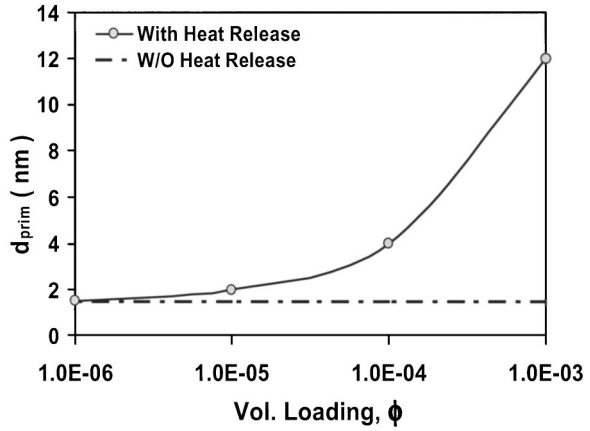

FIG. 18. The effect of particle volume loading ($\phi = 10^{-3}, 10^{-4}, 10^{-5}, 10^{-6}$) on the prediction of primary particle sizes (d_{prim}) for titania nanoparticle coalescence, $T_g = 1600$ K, and gas pressure, $P_g = 101$ kPa (1 atm). A primary particle size without heat release effect has also been indicated.

The Monte Carlo model indicates that under certain growth conditions of gas temperature, particle volume loading, and background pressure, particles may experience highly elevated temperatures. This occurs when the characteristic time for coalescence is much smaller than the characteristic collision and cooling time. This can be accomplished through a decrease in pressure that lowers the heat loss from the hot particle as it coalesces and, therefore, enhances its sintering rate through the exponential dependence of the diffusion coefficient on the particle temperature. Alternatively, one can increase the volume fraction to hasten up the collision rate under conditions where the sintering rate is faster than the collision rate. In this process we decrease the time interval between when a particle is sintered (and hot) and undergoing quenching, and when another heat generating collision/coalescence occurs, to further enhance the coalescence process.

These criterion reveal that heat generation during a typical nonisothermal coalescence phenomenon has a very strong effect on the coalescing dynamics of nanoparticles and, thereby, also plays a significant role in determining the growth rates of primary particles, both in terms of their morphology and size. From the present study, we may conclude that during typical nanoparticle coalescence phenomenon, increased volume loading and decreased background gas pressure results in enhanced primary particle sizes and growth rates, particularly in the regime when heat generation from coalescing nanoparticles is significant, i.e., when $\tau_f < \tau_c < \tau_{\text{cool}}$.

ACKNOWLEDGMENTS

Support for this work comes from the Army DURINT Center for NanoEnergetics Research, the Army High Performance Computing Research Center DAAD19-01-2-0014, and the Minnesota Super-Computer Center.

[1] S. E. Pratsinis, Prog. Energy Combust. Sci. **24**, 197 (1998).
[2] M. M. Mench, K. K. Kuo, C. L. Yeh, and Y. C. Lu, Combust. Sci. Technol. **135**, 269 (1998).
[3] N. Ichinose, Y. Ozaki, and S. Kashu, *Superfine Particle Technology* (Springer-Verlag, Berlin, 1992).
[4] C. M. Megaridis and R. A. Dobbins, Combust. Sci. Technol. **71**, 95 (1990).
[5] S. K. Friedlander, *Smoke, Dust and Haze*, 1st ed. (Wiley, New York, 1977) and 2nd ed. (Oxford University Press, New York, 2000).
[6] K. E. J. Lehtinen and M. R. Zachariah, Phys. Rev. B **63**, 205402 (2001).
[7] R. S. Windeler, K. E. J. Lehtinen, and S. K. Friedlander, Aerosol Sci. Technol. **27**, 191 (1997).
[8] R. S. Windeler, S. K. Friedlander, and K. E. J. Lehtinen, Aerosol Sci. Technol. **27**, 174 (1997).
[9] T. Seto, M. Shimada, and K. Okuyama, Aerosol Sci. Technol. **23**, 183 (1995).
[10] S. Tsantilis and S. E. Pratsinis, AIChE J. **46**, 407 (2000).
[11] S. H. Ehrman, S. K. Friedlander, and M. R. Zachariah, J. Aerosol Sci. **29**, 687 (1998).
[12] I. V. Schwiegert, K. E. J. Lehtinen, M. J. Carrier, and M. R. Zachariah, Phys. Rev. B **65**, 235410 (2002).
[13] F. E. Kruis, K. A. Kusters, and S. E. Pratsinis, Aerosol Sci. Technol. **19**, 514 (1993).
[14] Y. Xing and D. E. Rosner, J. Nanoparticle Res. **1**, 277 (1999).
[15] H. J. Freund and S. H. Bauer, J. Phys. Chem. **81**, 994 (1977).
[16] K. E. J. Lehtinen and M. R. Zachariah, J. Colloid Interface Sci. **242**, 314 (2001).

[17] M. R. Zachariah and M. J. Carrier, J. Aerosol Sci. **30**, 1139 (1999).
[18] D. E. Rosner and S. Yu, AIChE J. **47**, 545 (2001).
[19] F. E. Kruis, A. Maisels, and H. Fissan, AIChE J. **46**, 1735 (2000).
[20] Y. Efendiev and M. R. Zachariah, J. Colloid Interface Sci. **249**, 30 (2002).
[21] K. E. J. Lehtinen and M. R. Zachariah, J. Aerosol Sci. **33**, 357 (2002).
[22] M. R. Zachariah, M. J. Carrier, and E. Blasiten-Barojas, J. Phys. Chem. **100**, 14856 (1996).
[23] W. Koch and S. K. Friedlander, J. Colloid Interface Sci. **140**, 419 (1990).
[24] M. K. Wu, R. S. Windeler, C. K. R. Steiner, T. Bors, and S. K. Friedlander, Aerosol Sci. Technol. **19**, 527 (1993).
[25] C. L. Yaws, *Handbook of Vapor Pressure* (Gulf Publishing Co., Houston, 1994).
[26] G. V. Samsonov, *The Oxide Handbook* (IFI/Plenum, New York, 1973).
[27] P. Buffat and J. P. Borel, Phys. Rev. A **13**, 2287 (1976).
[28] P. Tandon and D. E. Rosner, J. Colloid Interface Sci. **213**, 273 (1999).
[29] T. Iida, H. Sakai, Y. Kita, and K. Murakami, High Temperature Mater. Process. **19**, 153 (2000).
[30] K. Hansen and E. E. B. Campbell, Phys. Rev. E **58**, 5477 (1998).
[31] S. Kumar and C. L. Tien, J. Heat Transfer **112**, 178 (1990).
[32] P. M. Tomchuk and B. P. Tomchuk, Zh. Eksp. Teor. Fiz. **112**, 661 (1997).
[33] I. S. Altman, D. Lee, J. Song, and M. Choi, Phys. Rev. E **64**, 052202 (2001).
[34] C. G. Bohren and D. R. Huffman, *Absorption and Scattering of Light by Small Particles* (Wiley, New York, 1983).
[35] J. Norris, Ann. Appl. Prob. **9**, 78 (1999).
[36] K. Liffman, J. Comput. Phys. **100**, 116 (1992).
[37] M. Smith and T. Matsoukas, Chem. Eng. Sci. **53**, 1777 (1998).
[38] M. Kostoglou and A. G. Konstandopoulos, J. Aerosol Sci. **32**, 1399 (2001).
[39] J. T. van Peborgh Gooch and M. Hounslow, AIChE J. **42**, 1864 (1996).
[40] D. T. Gillespie, J. Atmos. Sci. **32**, 1977 (1975).
[41] B. H. Shah, D. Ramkrishna, and J. D. Borwanker, AIChE J. **23**, 897 (1977).
[42] S. K. Friedlander and M. K. Wu, Phys. Rev. B **49**, 3622 (1994).
[43] S. Vemury, K. A. Kusters, and S. E. Pratsinis, J. Colloid Interface Sci. **165**, 53 (1994).
[44] R. M. German, *Sintering Theory and Practice* (Wiley, New York, 1996).
[45] R. C. Weast, *CRC Handbook of Chemistry and Physics* (CRC, Boca Raton, FL, 1989).
[46] M. Astier and P. Vergnon, J. Solid State Chem. **19**, 67 (1976).
[47] D. L. Martin, L. M. Raff, and D. L. Thompson, J. Chem. Phys. **92**, 5311 (1990).
[48] R. Seigel and J. R. Howell, *Thermal Radiation Heat Transfer*, 3rd ed. (Hemisphere, Washington, DC, 1992).